Title
A Ray Theory Imaging Algorithm for VSP Data

Authors
Eastwood, F.S.
Majer, E.L.
McEvilly, T.V.

Publication Date
1986-11-01

LBL-22597
Preprint

Lawrence Berkeley Laboratory
UNIVERSITY OF CALIFORNIA

EARTH SCIENCES DIVISION

Submitted to Geophysics

A Ray Theory Imaging Algorithm for VSP Data

F.S. Eastwood, E.L. Majer, and T.V. McEvilly

November 1986

Prepared for the U.S. Department of Energy under Contract Number DE-AC03-76SF00098.

DISCLAIMER

LBL-22597

A Ray Theory Imaging Algorithm for VSP Data

F.S. Eastwood, E.L. Majer, and T.V. McEvilly

Earth Sciences Division
Lawrence Berkeley Laboratory
University of California
Berkeley, CA 94720

This work was supported by the Director, Office of
Basic Energy Sciences, of the U.S. Department of Energy under
Contract No. DE-AC03-76SF00098.

A Ray Theory Imaging Algorithm for VSP Data

F. S. Eastwood, E. L. Majer, and T. V. McEvilly

Center for Computational Seismology, Lawrence Berkeley Laboratory
and
Department of Geology and Geophysics, University of California,
Berkeley, CA 94720

ABSTRACT

We present a ray-theoretical approach to the imaging of nonzero-offset vertical seismic profiling (VSP) data. The method is valid for arbitrary source-receiver geometries, including non-VSP geometries. It is also capable of correctly imaging reflectors in the presence of arbitrary two dimensional velocity variations. The algorithm is a noncoincident source and receiver generalization of 'event' or 'interface' migration of common midpoint (CMP) seismic reflection data. The method is applied to synthetic and real VSP data from a geothermal field in northern Japan to image a steeply dipping reflector.

Introduction

Imaging of VSP data has been discussed by Chang and McMechan (1986), and Whitmore and Lines (1986). These methods involve the extrapolation of the observed reflected wavefield at the borehole backward in time through the use of finite differencing schemes. The imaging condition may be derived by ray tracing (Chang and McMechan) or by using a forward propagating finite difference scheme (Whitmore and Lines) from the source location. Accurate results are

critically dependent on regular receiver spacing, fine spatial sampling, and noise-free traces.

The VSP imaging scheme discussed in this paper differs from the above algorithms in that it uses the ray method for both the extrapolation of the observed reflections back in time and also to determine the imaging condition. The method is completely general in that it will allow arbitrary coplanar source-receiver geometry, and arbitrary vertical and lateral velocity variations. Unlike other VSP imaging methods though, this method requires the 'picking' or timing of VSP reflections from the raw (unmigrated) data. In essence, the method discussed is the noncoincident source and receiver counterpart to 'event' or 'interface' migration of CDP reflection seismic data described by Sattlegger (1982).

The Algorithm

As with the method of Sattlegger, the identification of reflection arrivals is the first step in the implementation of our algorithm. Reflector segments and corresponding slownesses are identified from the raw VSP data. In the current implementation we estimate reflector slownesses along the borehole trajectory by fitting a cubic spline to the travel times. A basic ambiguity exists between energy that approaches the borehole from below and the left or from below and the right (for example) and the two are indistinguishable on the basis of travel times and slowness estimates derived from receivers within the borehole. An equivalent ambiguity does not exist for surface recordings because all energy is assumed to be arriving from within the earth (below). Either one or the other possibilities must be selected using independent information such as polarization studies of the particle motion or a priori knowledge of the likely location of the reflector.

The basic outline of the imaging algorithm is illustrated in Figure 1. At each receiver level the observed reflections are extrapolated backward in time (or away from the borehole) at the specified slowness using the ray tracing method described by Cerveny et al (1977). A point, B, is selected on the ray from the receiver, A, as a trial imaging location for the reflector. Initially, for example, we may select point B as being that point which is located an amount $T_{observed}/2$ from point A. The ray path, from point B to source location C is then computed using the two-point 'ray bending' method described by Julian and Gubbins (1977). In general $T_{AB}+T_{BC}$ will not equal $T_{observed}$. Therefore, we revise the coordinates of point B an amount $(\delta x, \delta z)$ using:

$$\delta T = T_{observed} - T = \left(\frac{\partial T}{\partial x}\right)_B \delta x + \left(\frac{\partial T}{\partial z}\right)_B \delta z \tag{1}$$

where

$$T = T_{AB} + T_{BC} \tag{2}$$

subject to the constraint that point B remain located on the ray emanating from point A. For small changes in δx and δz this constraint can be quantified as :

$$\delta x / \delta z = \left(\frac{\partial T_{AB}}{\partial x}\right)_B \Big/ \left(\frac{\partial T_{AB}}{\partial z}\right)_B \tag{3}$$

The partial derivitives are easily evaluated during the computation of the ray paths. Point B is revised iteratively until $T_{observed} - T$ is less than some predetermined threshold (for example, the timing uncertainty). Essentially we are adjusting point B, on ray AB, iteratively until the total calculated travel time, $T_{AB}+T_{BC}$ matches $T_{observed}$. In the tests we have conducted only 3 or 4 iterations at most are required. The entire procedure is repeated for the remaining receiver locations and the reflector is then defined by the collection of imaging locations.

Application to Synthetic Data

The algorithm described in the previous section is applied to synthetic data. The data were generated using a finite difference approximation to the scalar wave equation, with absorbing boundary conditions, similar to the programs described by McMechan (1985) or Alford et al (1974). The model approximates the geometry of the Nigorikawa geothermal field located in northern Japan, which is the location of the actual shear wave VSP studied in the next section (see Figure 2). The high angle interface represents the edge of the Nigorikawa caldera. The low-velocity caldera fill is composed of Quaternary age deposits of unconsolidated ash and other volcanic debris. The surrounding country rock is composed of Neogene to Miocene age tuffs, andesites, and cherts (K. Sato, personal communication). The velocities annotated are representitive of the observed shear wave velocities in the area. The finite difference grid used was 300 by 300 nodes, with a 5 m interval. The source waveform had a time history of the derivitive of a gaussian function with dominant frequency of 3 Hz, centered at time zero. The source was located on the surface 100 m from the well location.

Figure 3 illustrates the evolution of the wavefield after 1.14 seconds. A reflection from the high angle interface is evident. Using the ray theory algorithm we attempt to image this reflector. The first 2.5 sec of the resultant synthetic VSP data are illustrated in Figure 4.

The measured travel times for the caldera reflection are illustrated in Figure 5. The reflection was not picked at all VSP receiver levels due to contamination by the direct arrival, for deep receivers, or the free surface reflection, for the shallow receivers. The event was timed at the zero crossings of the waveform to the nearest 8 msec. The vertical slowness of the reflection, as determined from a cubic spline fit, is illustrated in Figure 6.

The imaging algorithm was applied to the travel times and slownesses in Figures 5 and 6. Figure 7 illustrates the resultant raypaths, and for comparison purposes the actual caldera edge (used in the forward modelling procedure) is included. The reflection point of each ray falls on or near the actual caldera edge thus demonstrating success in the test of our synthetic data. The results are consistent within the time step size of the finite difference scheme of 8 msec, which roughly translates into a radius of uncertainty of 8 m. Undoubtably some smoothing of the arrival times, and consequently the slowness estimates would provide a more evenly sampled image of the reflector.

Application to Real Data

The algorithm was applied to actual VSP data from a well in the Nigorikawa geothermal field in northern Japan. A shear wave vibrator and a 3 component (nonoriented) borehole tool were used. The baseplate of the vibrator was oriented so motion was in the plane of the section, ie. an SV source. The vertical component waveforms are shown in Figure 8. The data were recorded in a deviated well and are of erratic quality. The VSP imaging techniques of Chang and McMechan or Whitmore and Lines are consequently inappropriate. Shear wave first arrival and reflection pick times are also presented. Polarization analysis of the three component recordings aided in the identification of the reflected arrival and confirmed that the reflected energy was arrriving from above and the right. First arrival times were used to define a velocity model for the imaging algorithm. A linear velocity gradient, $V(\ km\ /sec\ ) = 0.300 + 1.8Z(\ km\ )$, was selected as a reasonable fit to the main features of the first arrival travel times (see Figure 9). The reflection travel times are illustrated in Figure 10. Due to the noisy character of the data we used a linear fit to the travel times and, consequently, a constant slowness at all receiver levels (see

Figures 10 and 11).

The results are illustrated in Figure 12. The image points define a steeply dipping (75 to 80 degrees) reflector. The results are consistent with the observed outcrop of the caldera edge which is located approximately 0.75 km from the borehole and dipping toward the borehole.

The accuracy of the location of the reflector is difficult to estimate. The reflection travel times have been approximated by a linear function which may produce significant errors in both the computed travel times and slownesses. If we use the slowness estimates provided by the spline fit to the actual reflection travel times to estimate the slowness (see Figures 10 and 11) we obtain the image shown in Figure 13. The image points are much more diffuse than the constant slowness result (Figure 12). It is unrealistic to expect that the travel times and consequently the slowness esitmates are not contaminated by noise and thus we conclude that the constant slowness (smoothed) result provides a more realistic representation of the reflector.

As in most migration or 'imaging' schemes the choice of velocity model is critical in the positioning of the reflectors. As a sensitivity study, the procedure was repeated with linear gradients 25 % higher and 33 % lower than the optimal fit (see Figure 9). The surface velocities for these models have been adjusted to yield identical vertical travel times at 0.8 km depth. The resulting reflector segments compared in Figure 14 are steeper and farther from the borehole for the high gradient model, and conversely for the low gradient model. We conclude that the choice of linear gradient does not significantly alter the conclusion that there is a steeply dipping reflector lying less than 0.5 km from the borehole at approximately 0.75 km depth.

Discussion

We have developed and tested a ray theoretical algorithm for imaging reflectors when the velocity field contains arbitrary two dimensional variations. In our application to actual data we used a velocity model that was a function of depth only due to the lack of additional velocity control. The necessity of knowing the velocity field a priori is a drawback of all migration schemes. However the VSP recording geometry in conjunction with tomographic reconstruction techniques may provide a viable way of estimating the velocity field (for example see Peterson, et al. (1985)). If the velocity model is only a function of depth the least squares approach of Pujol, et al. (1985) is also applicable.

Several straightforward extensions to the method are also possible. We may include reflections observed from surface recordings with no modification to the method. The procedure may be extended to three dimensional geometries if it is possible to determine the azimuth of the arriving energy through the use of 3-component recordings. The imaging of correctly identified converted reflections is also possible if we prescribe a different velocity model for the AB and BC segments of the raypaths. The procedure can also be viewed as a modification of the method of aplanatic surfaces (Musgrave et al, 1967) if we replace the concept of 'reflection' image point by 'refraction' or 'diffraction' image point. For example, in the case of a salt proximity survey, the sediment velocity model would be used for ray segment AB and the salt dome velocity model for ray segment BC.

In short we have presented a method that can be used as an alternative to the migration schemes of Chang and McMechan or Whitmore and Lines. The method is particularily useful when data quality is poor, and the recording geometry is irregular. It also has potential

applications in three-dimensional geometries, in imaging converted reflections, and as an alternative to the method of aplanatic surfaces.

Acknowledgments

We wish to thank C. Araki, S. Takasugi and K. Sato of Geothermal Energy Research and Development Company for their help during the VSP survey conducted in the Nigorikawa geothermal field. This work was supported by the Director, Office of Basic Energy Sciences, of the U.S. Department of Energy under contract DE-AC03-76SF00098.

References

Alford, R. M., K. R. Kelly, and D. M. Boore, 1974, Accuracy of finite-difference modeling of the acoustic wave equation: Geophysics, **39** , 834-842.

Cerveny, V., I. A. Moloktov, and I. Psencik, 1977, Ray method in seismology: Univerzita Karlova.

Chang, W. F., and G. A. McMechan, 1986, Reverse-time migration of offset vertical seismic profiling data using the excitation-time imaging condition: Geophysics, **51** , 67-84.

Julian, B. R., and D. Gubbins, 1977, Three dimensional seismic ray tracing: J. Geophysics, **43** , 95-114.

McMechan, G. A., 1985, Synthetic finite-offset vertical seismic profiles for laterally varying media: Geophysics, **50** , 627-636.

Musgrave, A. W., Ed., 1967, Seismic refraction prospecting: Soc. Explor. Geophys.

Peterson, J. E., B. N. P. Paulsson, and T. V. McEvilly, 1985, Application of algebraic reconstruction techniques to crosshole seismic data: Geophysics, **50** , 1566-1580.

Pujol, J., R. Burridge, and S. B. Smithson, 1985, Velocity determination from offset vertical seismic profiling data: J. Geophys. Res., **90** , 1871-1880.

Sattlegger, J., 1982, Migration of seismic interfaces: Geophysical Prospecting, **30** , 71-85.

Whitmore, N. D., and L. R. Lines, 1986, Vertical seismic profiling depth migration of a salt dome flank: Geophysics, **51** , 1087-1109.

Figure Captions

Figure 1. Process flow for imaging algorithm

Figure 2. Velocity model for synthetic data. Velocities annotated are in units of km/sec.

Figure 3. Snaphot of wavefield generated from model in Figure 2. Identical vertical and horizontal scales. Note reflection from edge of caldera, well location is shown.

Figure 4. Synthetic VSP data generated from model in Figure 2. Horizontal timing line increment is 0.100 sec. Trace spacing increment is 50 m.

Figure 5. Reflection travel times from synthetic VSP data in Figure 4.

Figure 6. Reflection slownesses calculated from cubic spline fit of travel times in Figure 5.

Figure 7. Results of applying the imaging algorithm to the synthetic data. Notice that the reflection point of each ray falls on or near the actual caldera edge.

Figure 8. Actual shear wave VSP data from Nigorikawa caldera, Japan. Horizontal timing line increment is 0.100 sec. Trace spacing increment is 50 m. Also illustrated are the shear wave first arrival 'picks' (positive tick) and reflection arrivals (negative tick).

Figure 9. Actual first arrival travel times (from Figure 8) and predicted first arrival travel times for selected linear velocity gradient models.

Figure 10. Reflection travel times from Figure 8. Cubic spline fit and linear fit are also illustrated.

Figure 11. Reflection slownesses calculated from cubic spline fit and linear fit of travel times in Figure 10.

Figure 12. Results of applying the imaging algorithm to the actual VSP data from the Nigorikawa caldera. Reflection slowness determined from linear fit of travel times. The reflection points outline a steeply dipping reflector.

Figure 13. Results of applying the imaging algorithm to the actual VSP data from the Nigorikawa caldera. Reflection slowness determined from cubic spline fit of travel times.

Figure 14. Reflection image points that result from using diffferent linear velocity gradients.

IMAGING ALGORITHM

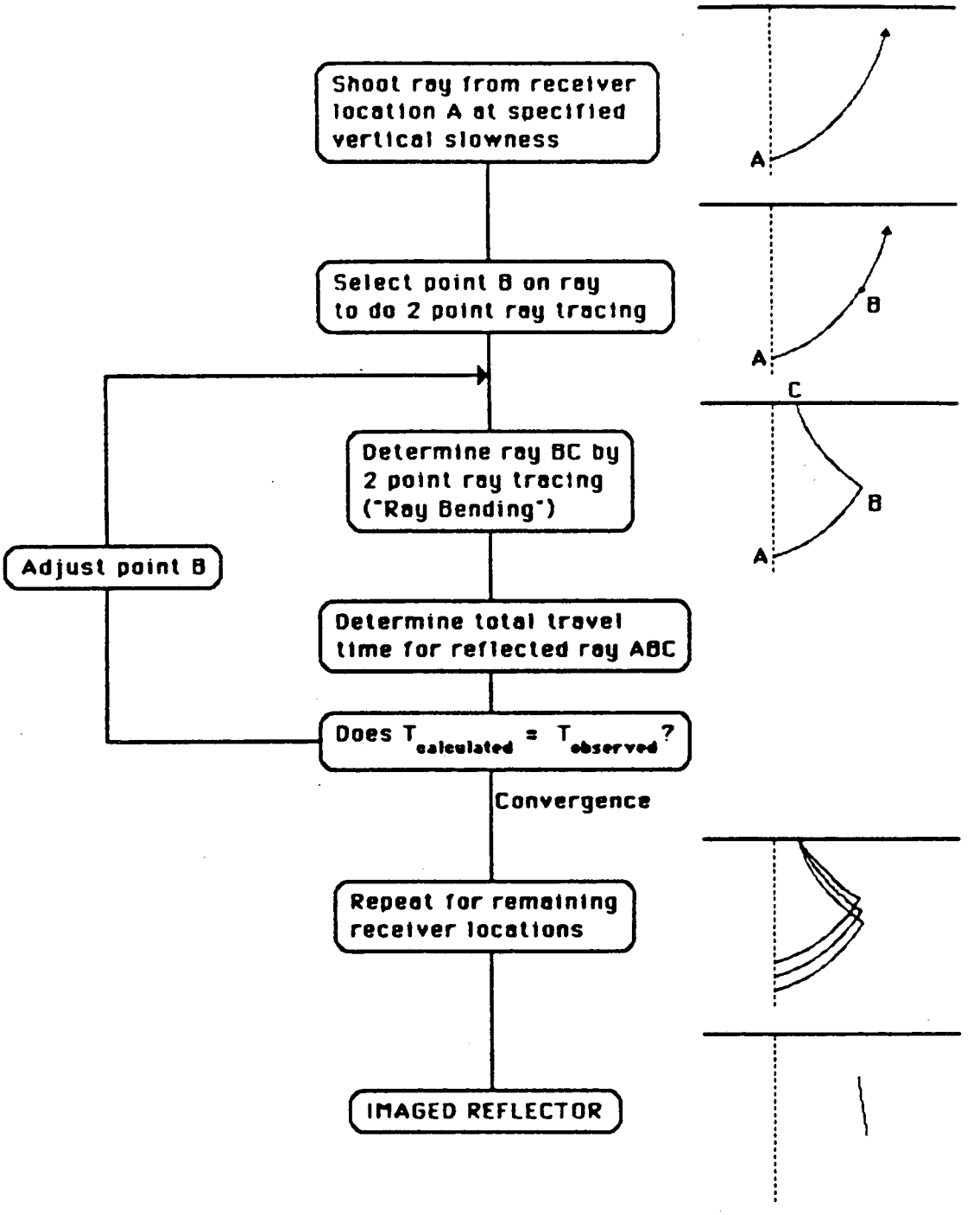

XBL 8611-4425

FIGURE 1

MODEL FOR SYNTHETIC DATA

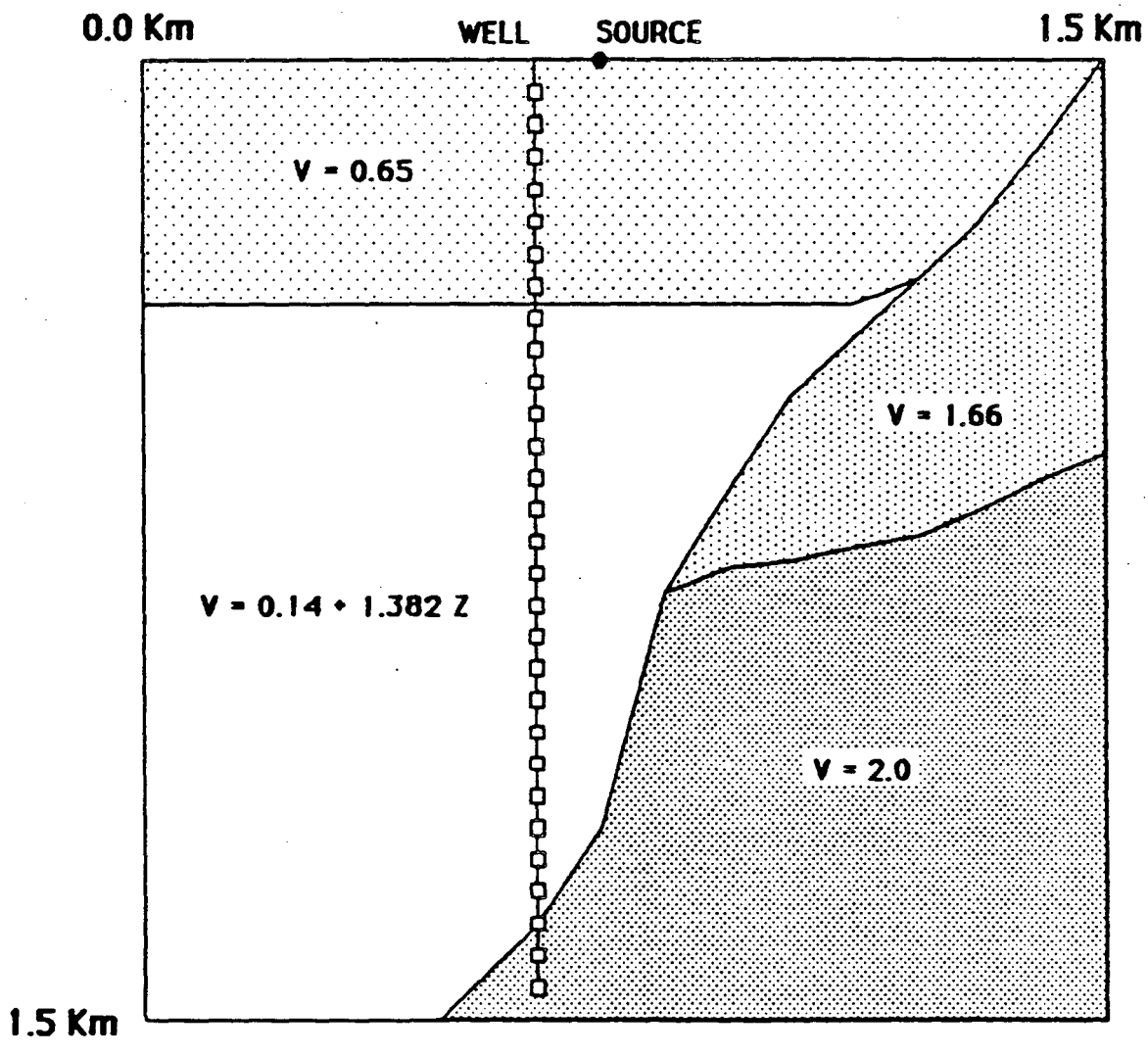

XBL 8611-4424

FIGURE 2

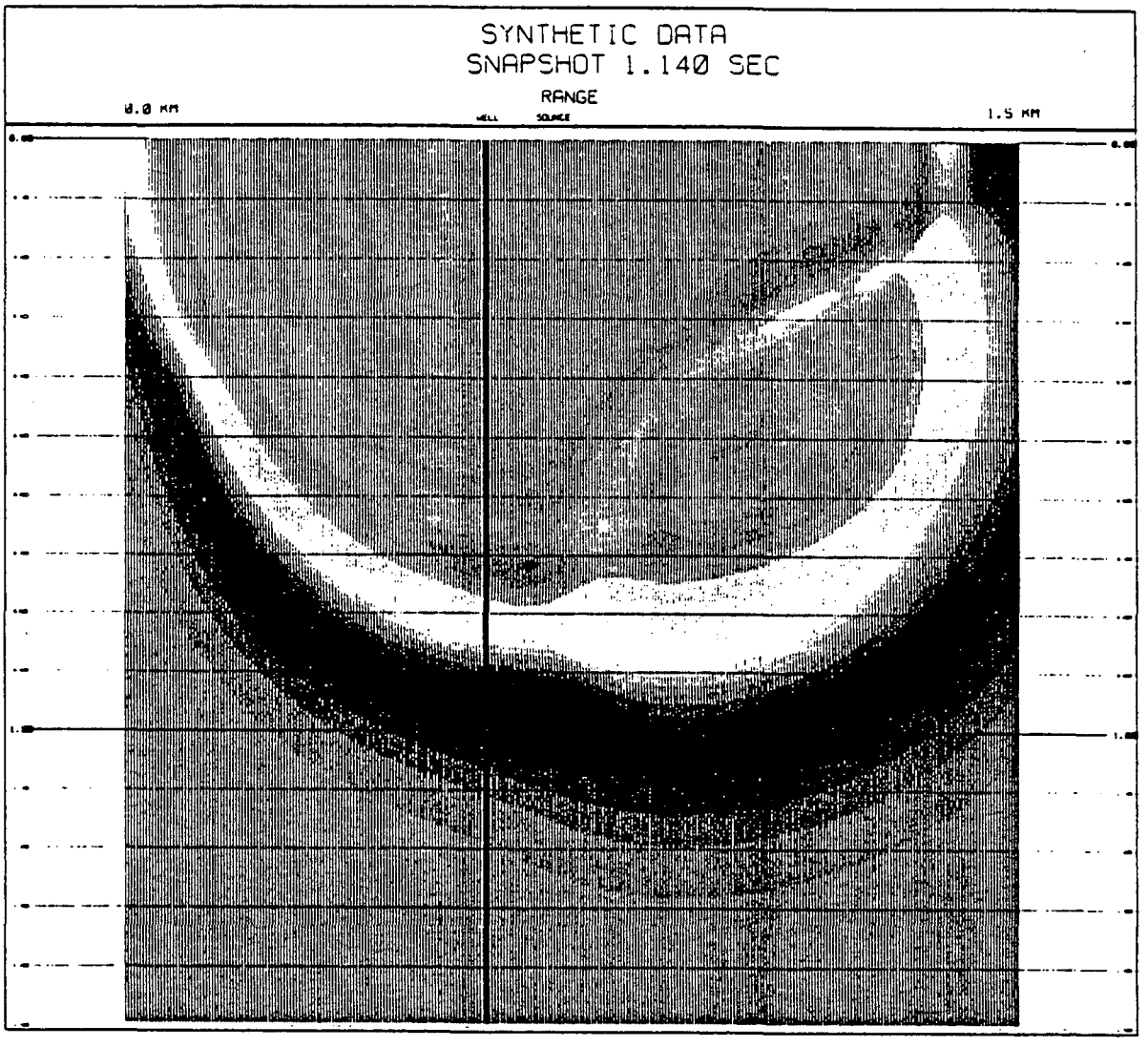

XBL 8611-4427

FIGURE 3

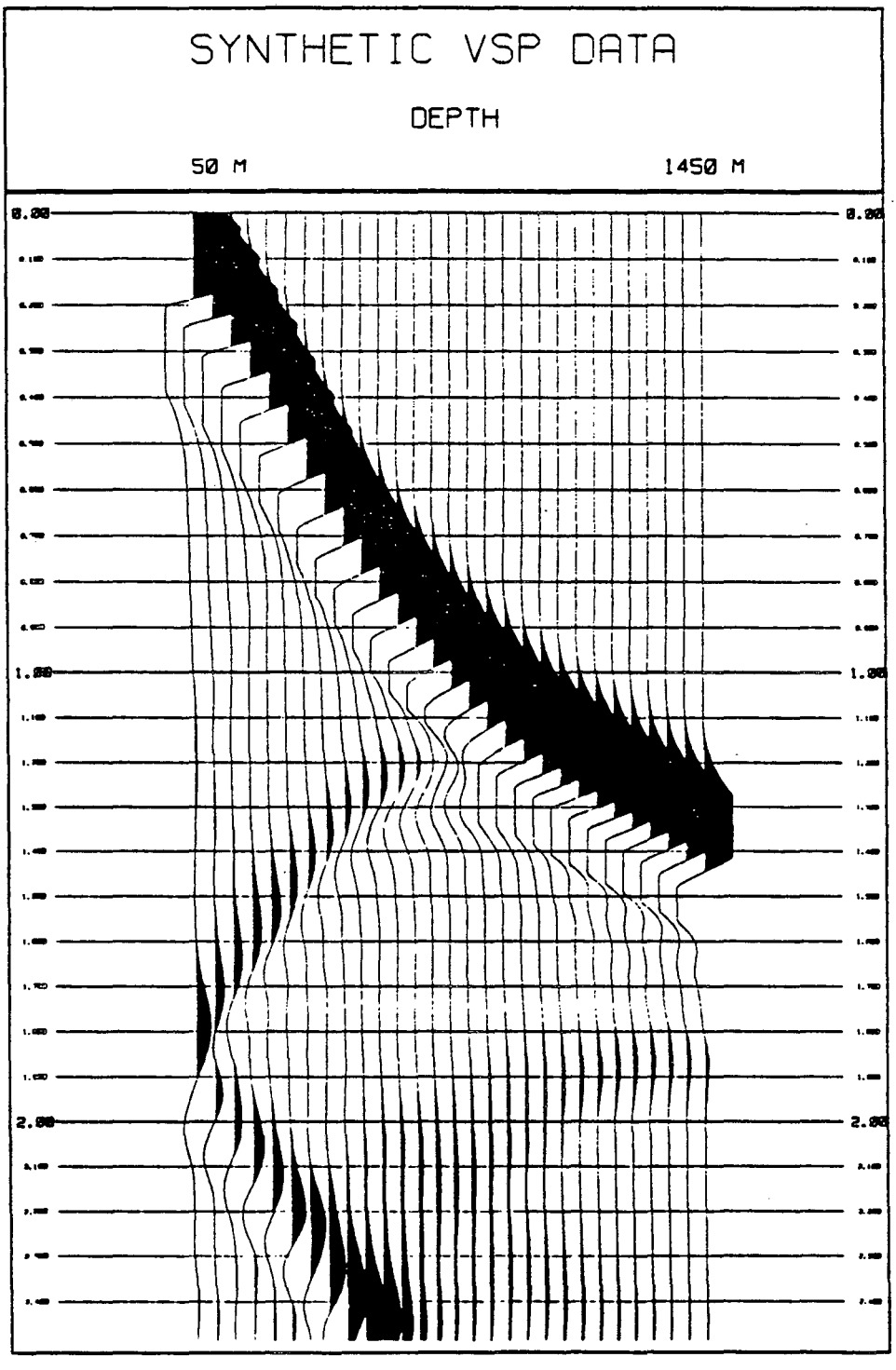

XBL 8611-4426

FIGURE 4

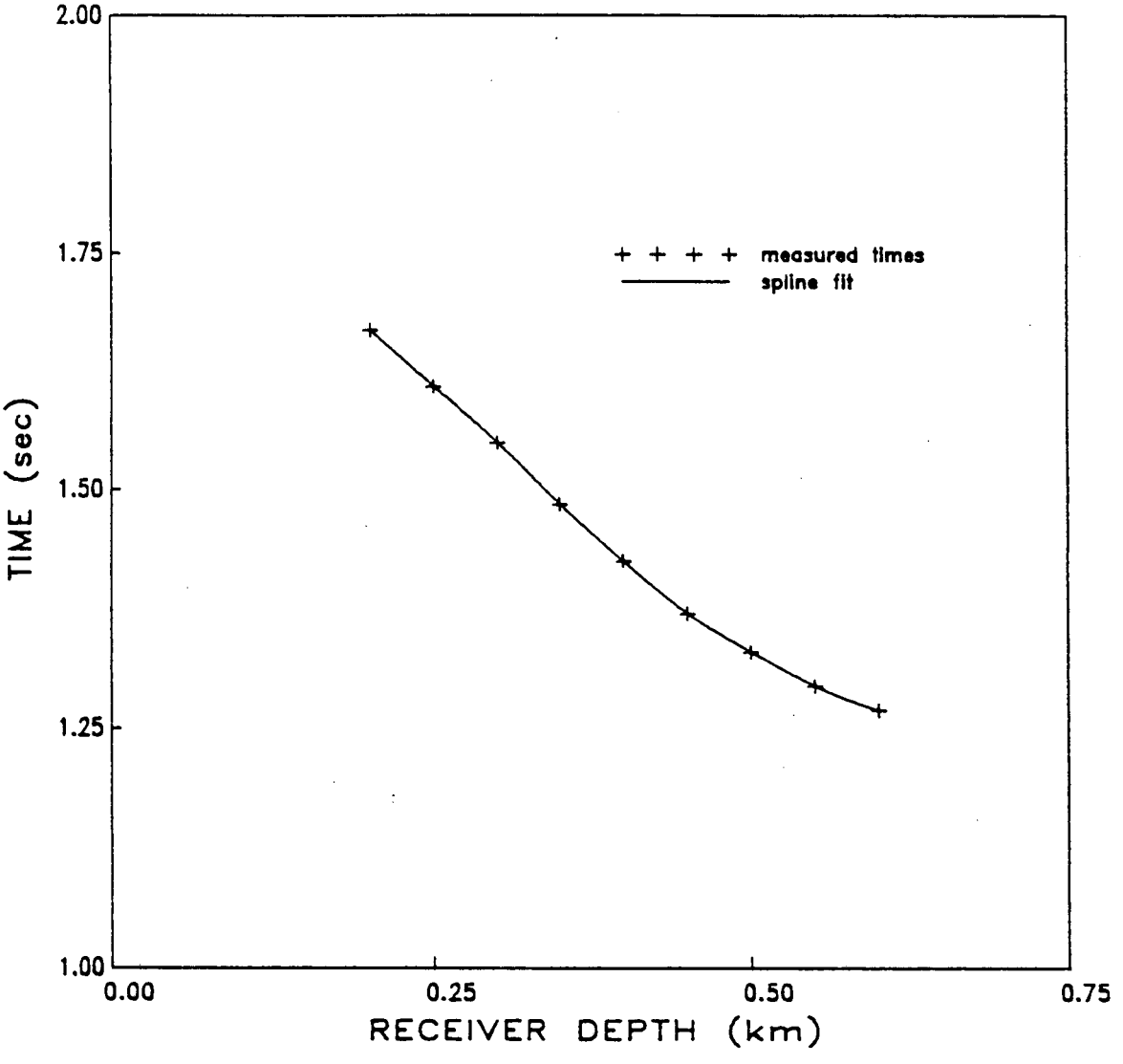

XBL 8611-4423

FIGURE 5

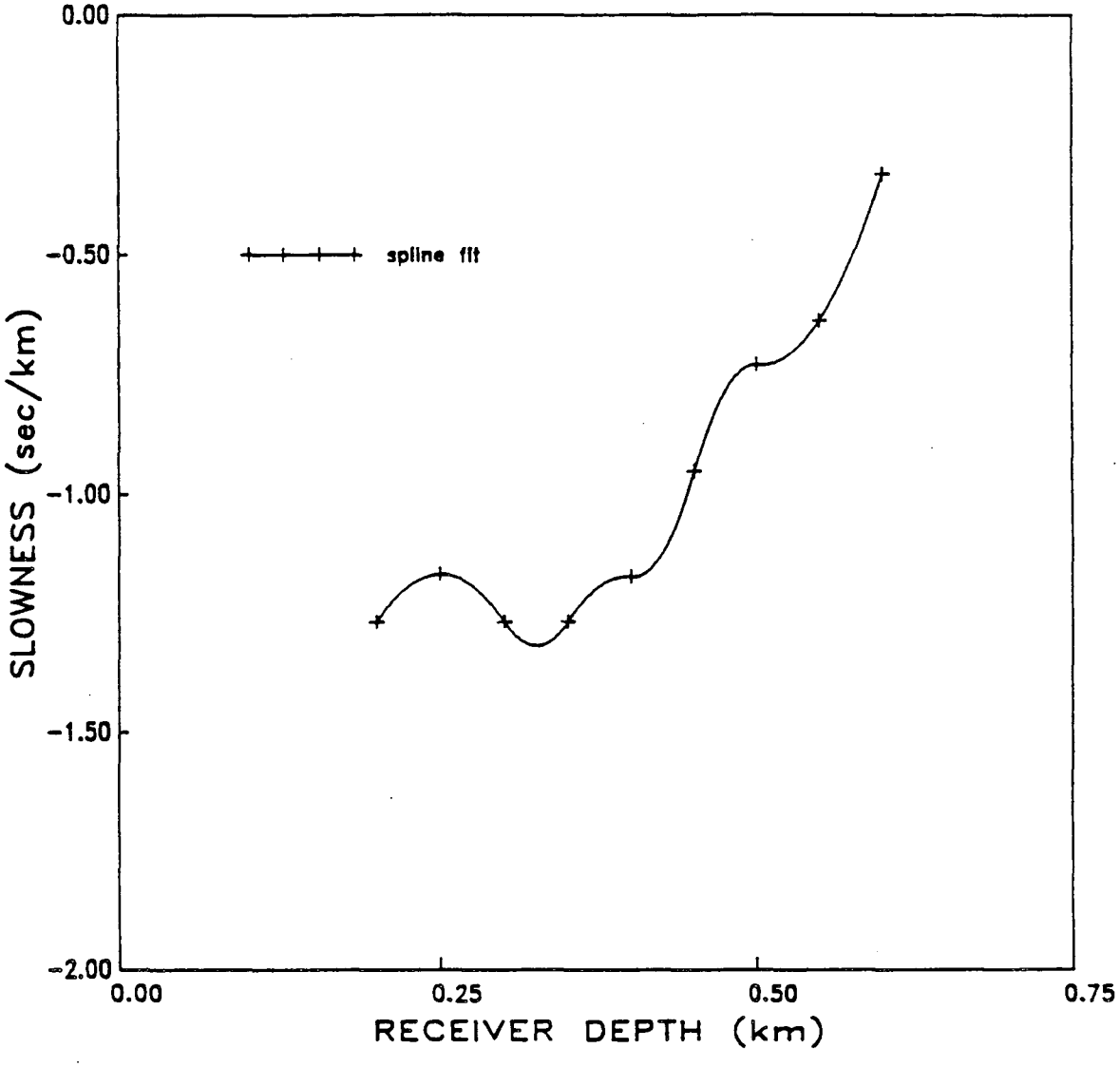

XBL 8611-4422

FIGURE 6

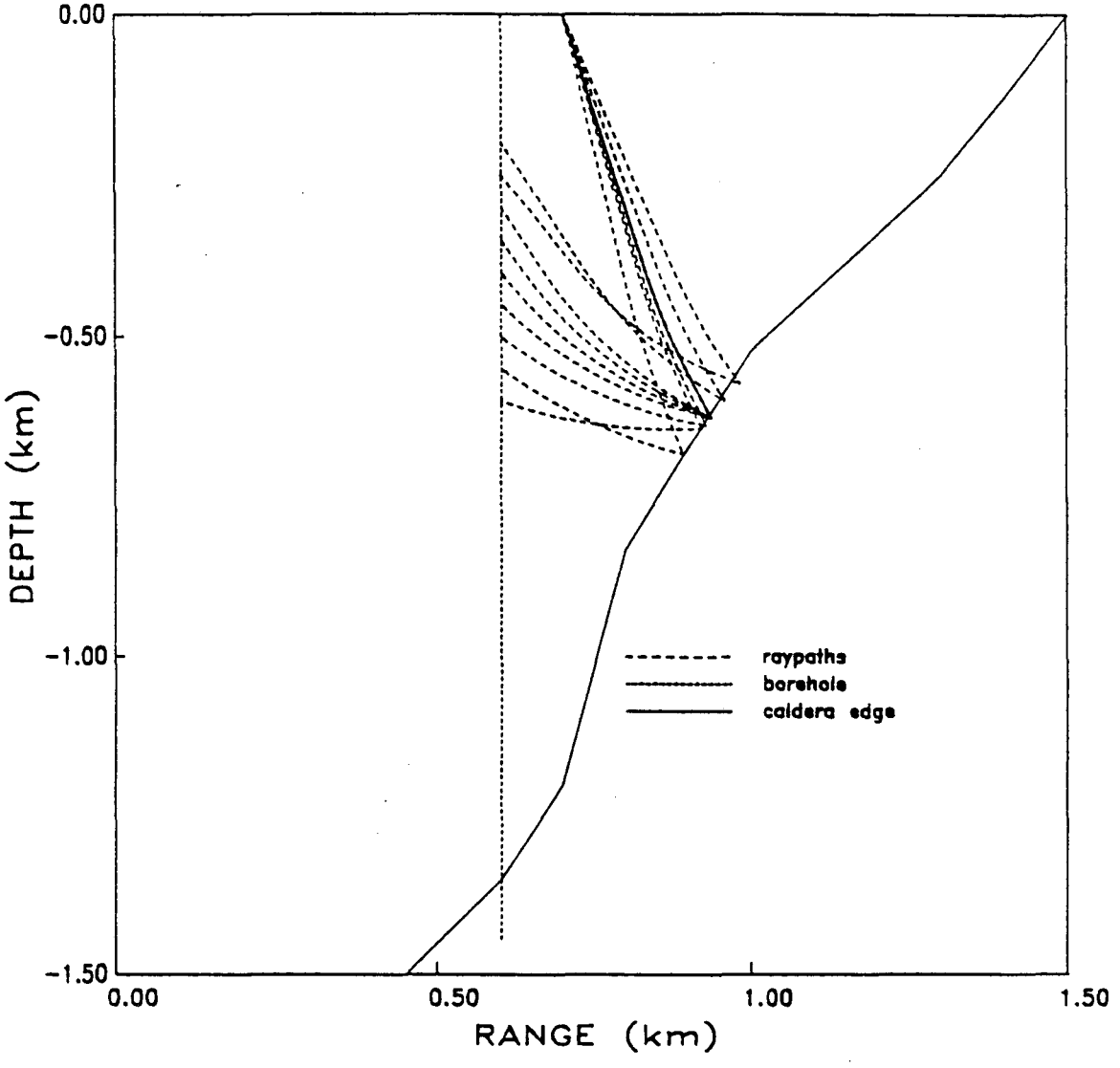

XBL 8611-4420

FIGURE 7

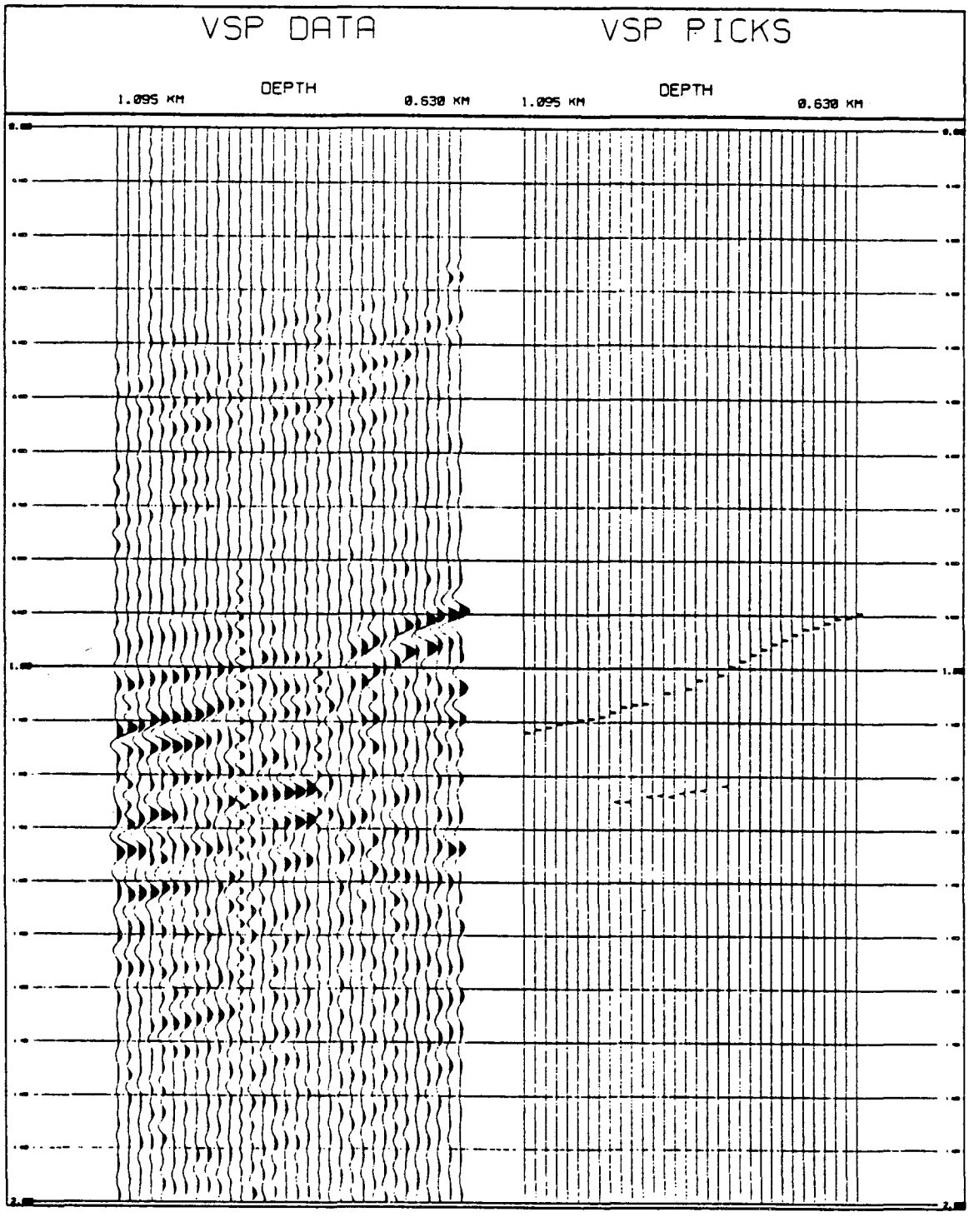

XBL 8611-4428

FIGURE 8

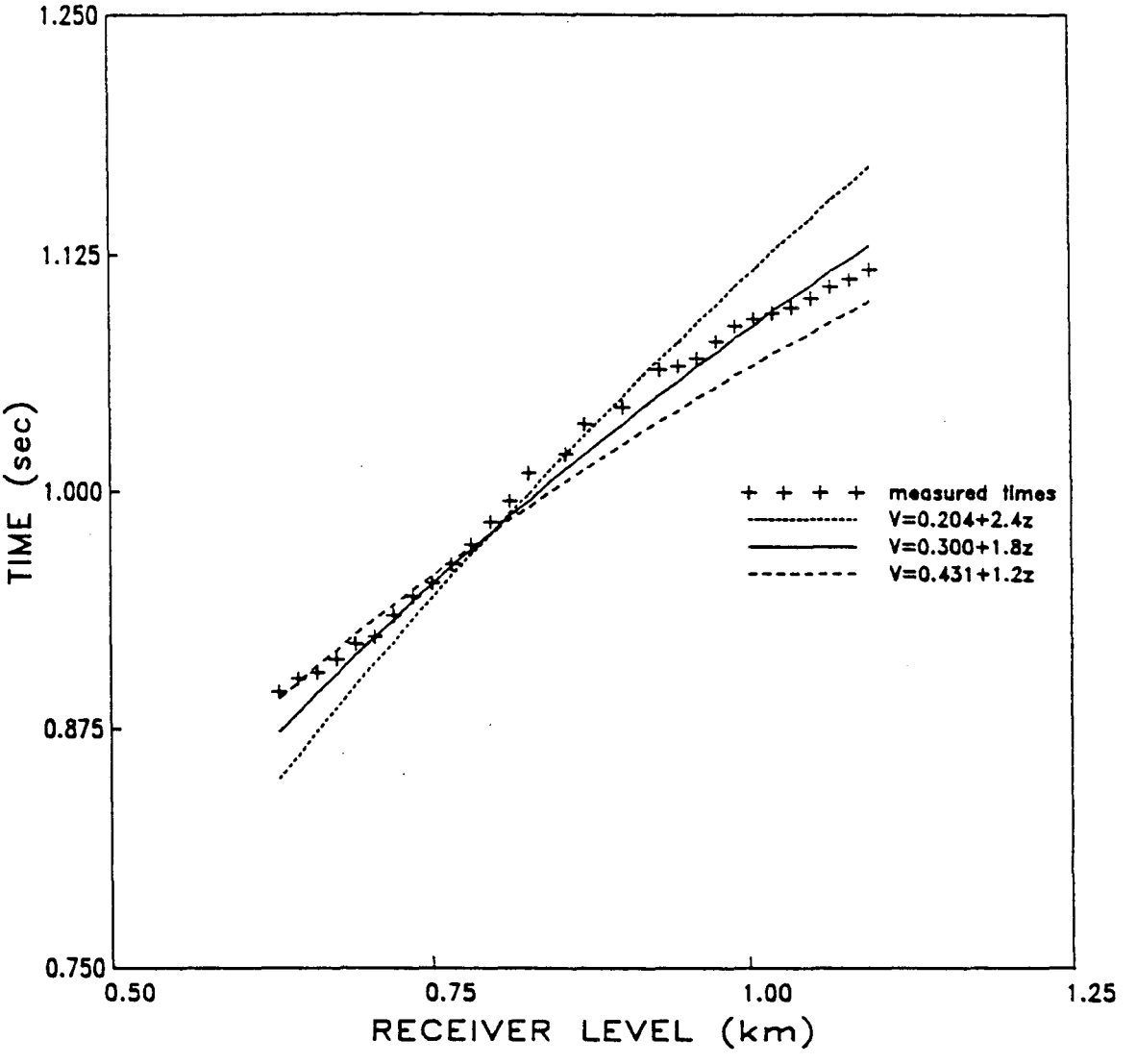

XBL 8611-4421

FIGURE 9

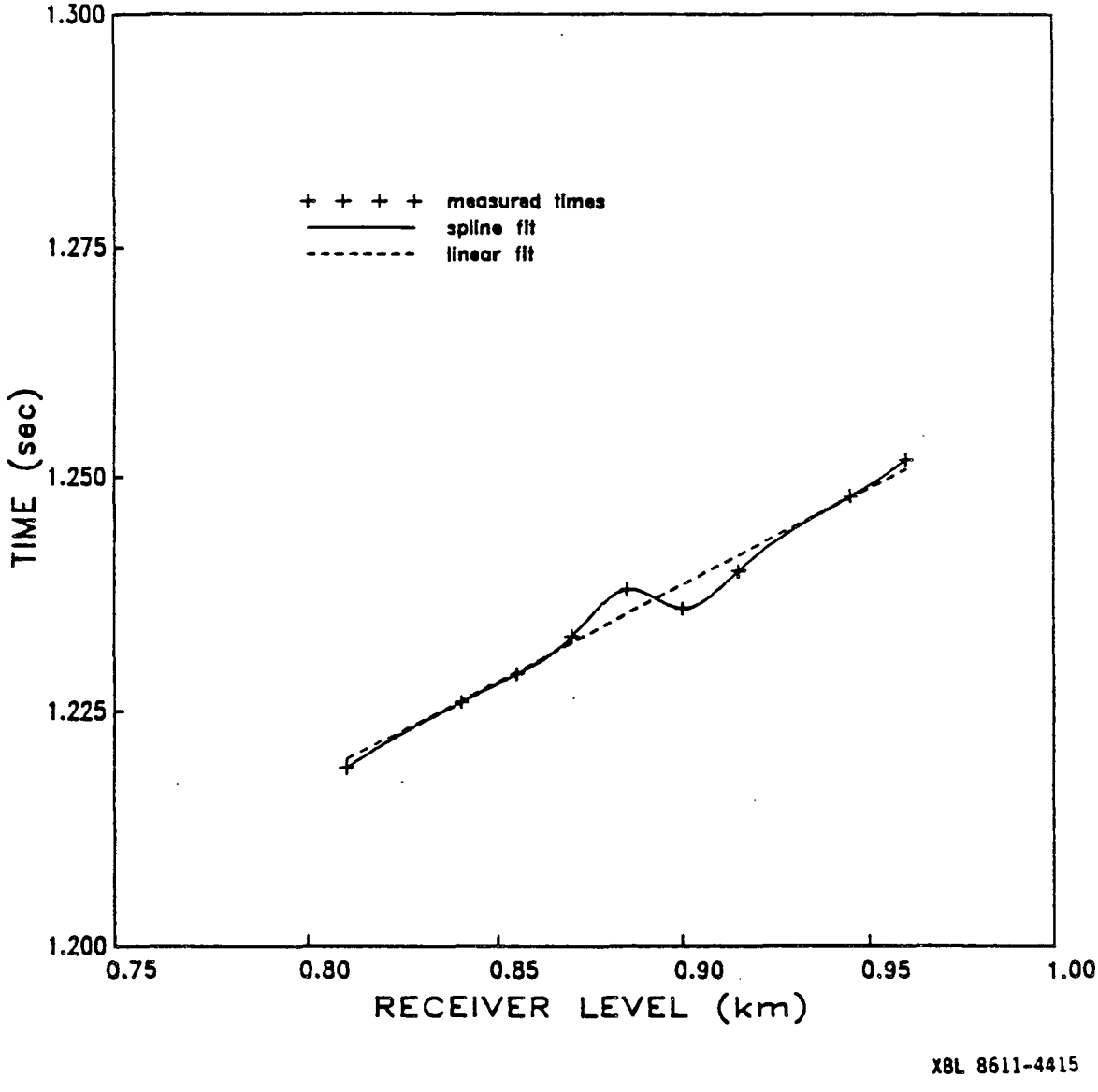
1.300
1.275
1.250
1.225
1.200
TIME (sec)
+ + + + measured times
spline fit
linear fit
0.75
0.80
0.85
0.90
0.95
1.00
RECEIVER LEVEL (km)
XBL 8611-4415

FIGURE 10

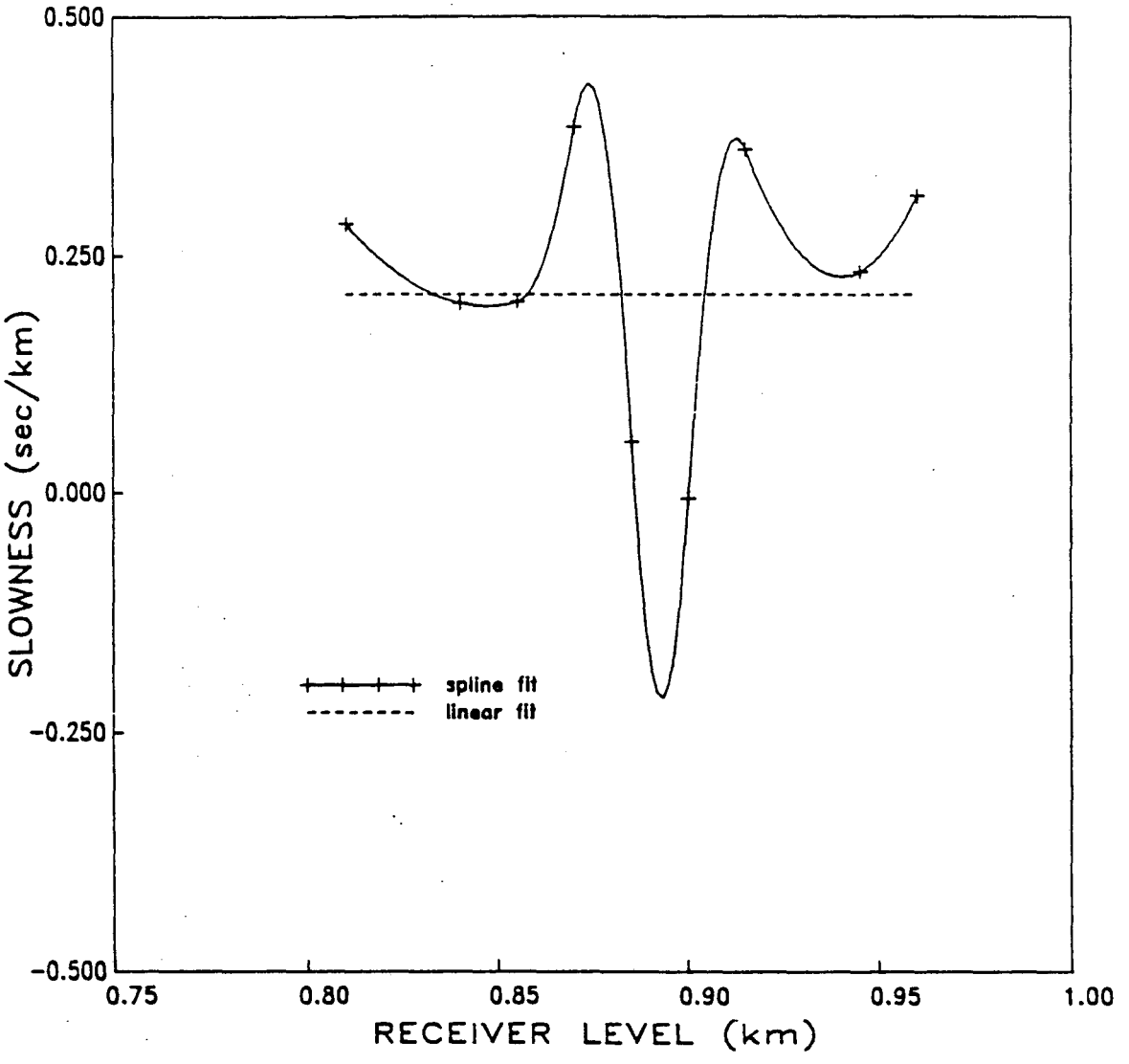

XBL 8611-4416

FIGURE 11

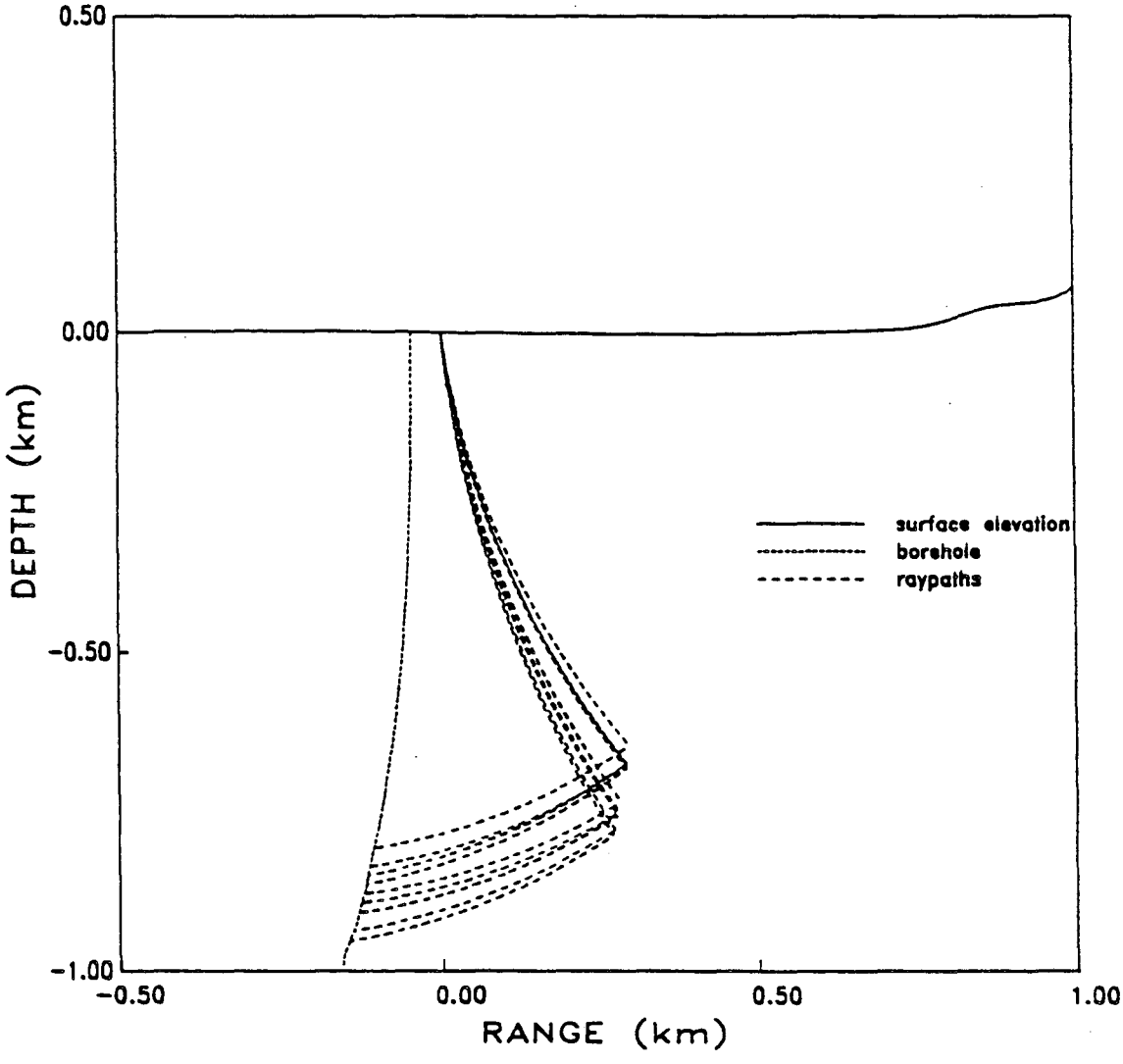

XBL 8611-4417

FIGURE 12

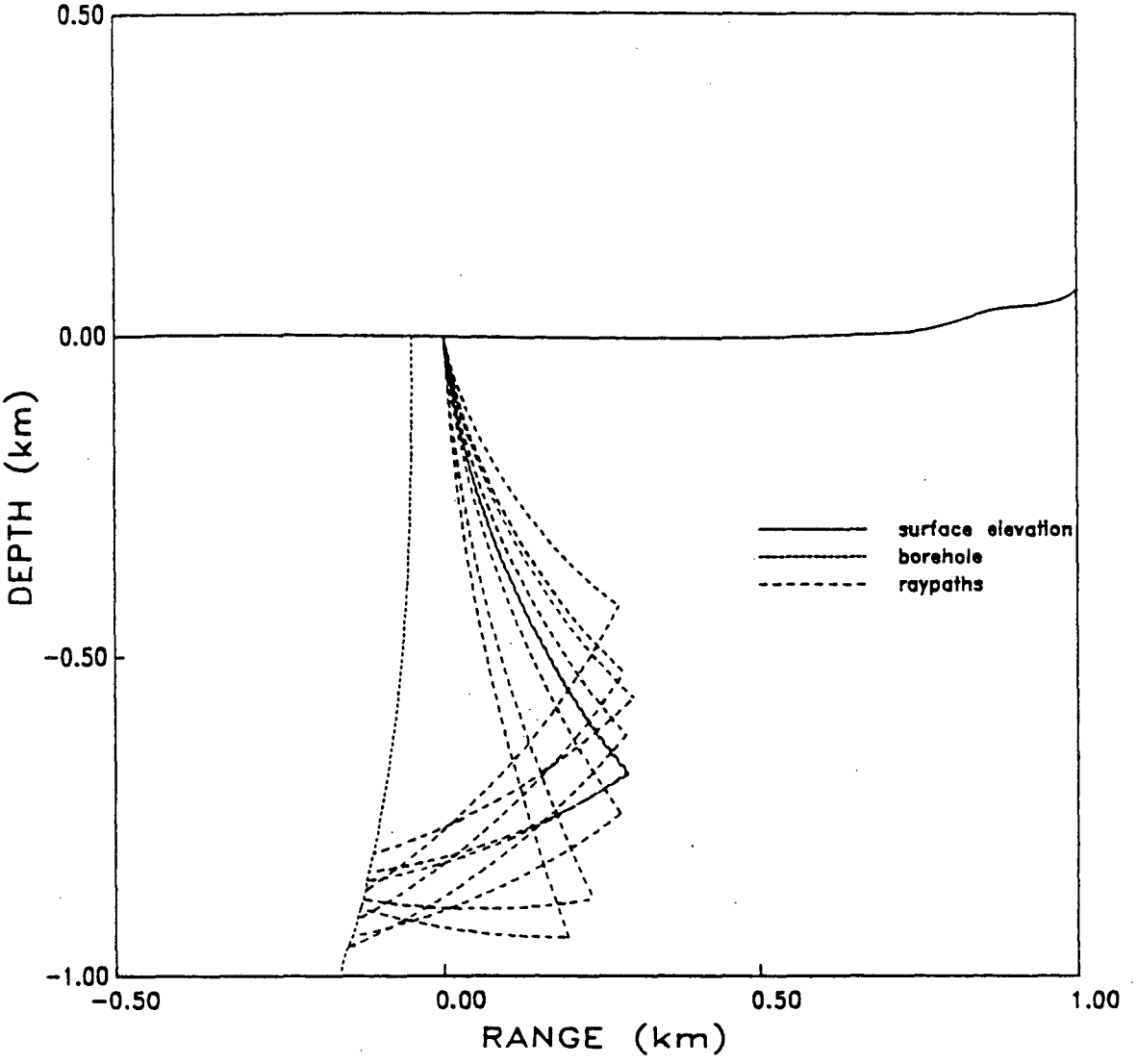
0.50
0.00
-0.50
-1.00
DEPTH (km)
-0.50
0.00
0.50
1.00
RANGE (km)
surface elevation
borehole
raypaths
XBL 8611-4418

FIGURE 13

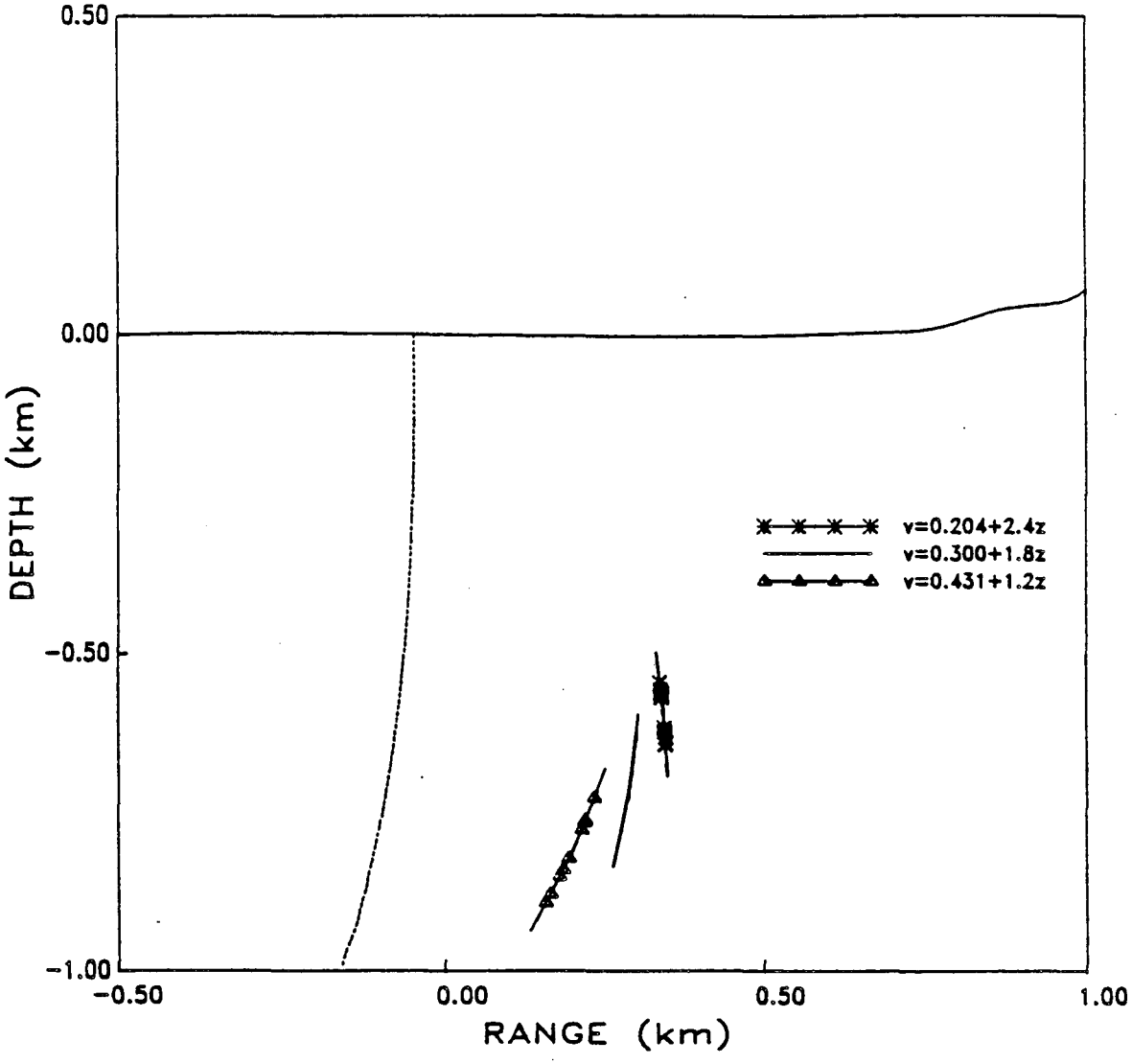

XBL 8611-4419

FIGURE 14

LAWRENCE BERKELEY LABORATORY
UNIVERSITY OF CALIFORNIA
INFORMATION RESOURCES DEPARTMENT
BERKELEY, CALIFORNIA 94720